DOI: https://doi.org/10.67897/njma.2021.aiaqnf8x



Nigerian Journal of Mathematics and Applications
Volume **31**, (2021), 77 – 96. *Printed by Unilorin press*
©*Nig. J. Math. Appl.* *http : //www.njmaman.com*

Effect of Brownian Motion and Thermophoresis on Heat and Mass Transfer of a Three- Dimensional Casson Fluid Flow Over a Stretching Sheet with Velocity Slip

A. S. Odesola, I. O. Abiala* and O. J. Fenuga

Abstract

This paper provides a numerical investigation on the effect of Brownian motion on the heat and mass transfer of a steady laminar MHD three-dimensional, Casson fluid flow over a surface which is stretched linearly in two lateral direction with convective surface boundary conditions. The governing Partial Differential Equations of the flow are transformed into a highly nonlinear coupled Ordinary Differential Equations (ODEs) consisting of continuity, momentum, energy and concentration equations via a suitable similarity variables. The resulting system of ODEs are solved using Finite Element Methods (FEM). The influence of the embedded parameters such as Prandtl, Porosity, thermal radiation, Brownian motion, Thermophoresis, Lewis number, Biot number are presented on the velocity, temperature and concentration. The effects of local skin friction coefficients, local Nusselt and Sherwood numbers are also obtained and presented. The result obtained favourably agreed with the existing ones.

Received: 18/09/2021, Accepted: 13/11/2021, Revised: 21/11/2021. * Corresponding author.
2020 *Mathematics Subject Classification.* 60J65 & 76M10.
Keywords and phrases. Brownian motion, Casson fluid, Convective boundary conditions, Finite Element Method, Heat and Mass transfer, MHD, Porosity, Stretching sheet, Thermal Radiation
Department of Mathematics, University of Lagos, Akoka, Lagos, Nigeria
E-mails of the corresponding author: iabiala@unilag.edu.ng, sotontop@yahoo.com
ORCID of the corresponding author: 0000-0001-9721-3499

1. Introduction

The present century has a better understanding of the principles of fluid dynamics and adopted it to many practical problems. Most of the problems in fluid dynamics are inherently nonlinear. So, these problems or phenomena are modelled by ordinary or partial differential equations. Solutions of these partial differential equations are important in predicting the future states of the problem phenomena under the study. It is well known fact that the fluids that appear in industrial and engineering processes are mostly non – Newtonian fluids [1].
The flow application of non – Newtonian fluids are evident in polymer processing, wire and fibre coating, heat exchangers, extrusion process, chemical processing equipment, to mention a few [2]. Combining heat transfer with the concept of stretching flow is vital in these areas of application. Non – Newtonian fluid exhibits nonlinear relationship between the shear stress and rate of shear strain [3]. It has attracted the attention of new researchers due to their huge range of practical applications in engineering, science and industries ([4] & [5]).
The materials that falls into the category of non-Newtonian fluid include sugar solution, colloidal and suspension solution and honey lubricants. The properties of such materials cannot be explored by simple Navier Stokes equations, therefore various kinds of non-Newtonian fluid models depending on different physical characteristics are developed, such as the Casson fluid, Jeffrey fluid, Maxwell fluid, Williamsom, Micropolar, and Nanofluid ([1], & [6]-[10]). In the category of non – Newtonian fluid, Casson has a distinctive features [4]. Human blood, jelly, honey, concentrated fruit juices, tomato sauces are some examples of Casson fluid [5].
The study of heat transfer in the stretched flow is important because of its extensive application in chemical engineering. Several processes in chemical engineering including metallurgical process and polymer extrusion process involved cooling of molten liquid being stretched into a cooling system, glass fibre and paper production ([8]-[11]). The quality and final product formation in such processes are dependent on the rate of cooling and stretching [12]. The heat transportation analysis in view of the non-Newtonian fluids have achieved a great significance in technology and science applications like production of synthetic liquids, electro rheological liquid, biological liquids movement, plastic products manufacturing through extrusion, chemical in district (heating/cooling) [13]. Casson fluid is classified as the most popular non – Newtonian fluids which has several applications in food processing, metallurgy, drilling operations and bio – engineering operations [3]. Earlier, Nadeem and others [4] discussed the MHD three-dimensional Casson fluid flow past a porous linearly stretching sheet. It was obtained that the porosity parameter, Casson fluid parameter and magnetic parameter reduces the momentum boundary layer thickness in both directions. [14] studied an unsteady MHD Casson fluid flow over a vertical cone and flat plate with non-uniform heat

source/sink and the results indicate that an increase in Casson fluid parameter is found to decelerate the fluid flow by increasing the plastic dynamic viscosity whereas it enhances the shear stress in flow regime. [15] studied the unsteady magnetohydrodynamic free flow of a Casson fluid over an oscillating vertical plate with constant wall temperature. Mahanta and Shaw [3] investigated the problem of a magnetohydrodynamic three dimensional Casson fluid flow past a porous linearly stretching sheet. The spectral relaxation Method (SRM) was used to solve the governing equations. [16] considered the analysis of three dimensional MHD flow of couple stress Casson fluid past an unsteady stretching surface with the effect of chemical reaction and convective boundary conditions. [13] elaborated the Soret-Dufour characteristics in mixed convective radiated Casson fluid flow by exponentially heated surface, the result signifies the characteristics of temperature corresponding to convective and radiation values. This work examines the effect of Brownian motion and thermophoresis on heat and mass transfer of MHD three-dimensional Casson fluid over a linearly stretching sheet with velocity slip through a porous medium and solved numerically using Finite Element Method (FEM).

2. Mathematical Analysis

We consider a steady, three- dimensional, viscous, incompressible, laminar MHD boundary layer Casson fluid flow, of a conducting heat and mass transfer over a stretching sheet through porous medium which is continuously stretched along xy-plane, while the fluid is situated at $z = 0$. It is also assumed that u, v and $w$are the velocity component of x, y and z-directions respectively. A constant induced magnetic field of strength B_0 is applied perpendicular to the stretching sheet in the z- direction and the effects of induced magnetic field is negligible since the magnetic Reynolds number is assumed to be small. The flow is caused by the stretching of the sheet that moves in its own plane with the surface velocity$u = ax + \gamma\frac{\partial u}{\partial z}$, $v = by + \gamma\frac{\partial v}{\partial z}$, and $w = 0$,where a, b (stretching rate) are positive constants. The fluid has no lateral motion at $z \to \infty$, the effects of thermal radiation and heat generation are taken into consideration.

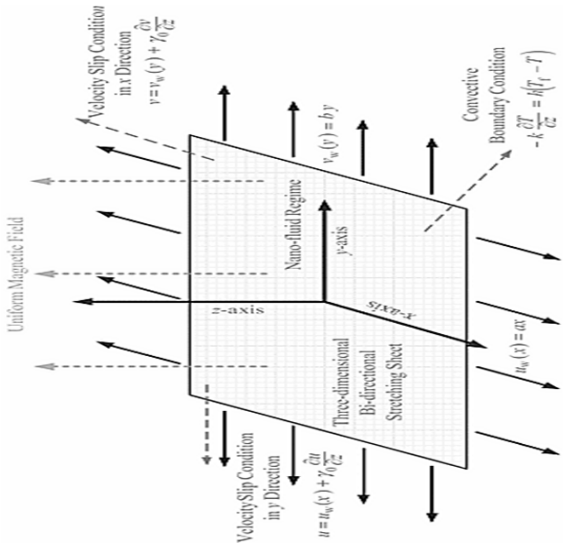


Figure 1: Physical Model and Coordinate System

The constitutive equation of state for an isotropic and incompressible Casson fluid is as follows ([16]-[20]):

$$\tau_{ij} = \begin{cases} 2\left(\mu_B + \frac{P_Z}{\sqrt{2\pi}}\right)e_{ij}, \pi > \pi_c \\ 2\left(\mu_B + \frac{P_Z}{\sqrt{2\pi_c}}\right)e_{ij}, \pi < \pi_c \end{cases} \tag{1}$$

where τ_{ij} is the $(i,j)th$ component of the stress tensor, $\mu_B$is the plastic dynamic viscosity of the non-Newtonian fluid, P_Z is the yield stress of the fluid, π is the product of the component of deformation rate with itself ($\pi = e_{ij}e_{ij}$), e_{ij} is the component of deformation rate, π_c is the critical value of product based on non-Newtonian model, $\beta = \mu_B\sqrt{2\pi_c}/P_z$ is the Casson parameter. Under the above assumptions, using the Oberbeck Boussinesq and boundary layer approximations, the governing equations describing the continuity, momentum, energy and concentration can be written in Cartesian coordinates as follows:

$$\frac{\partial u}{\partial x} + \frac{\partial v}{\partial y} + \frac{\partial w}{\partial z} = 0 \tag{2}$$

$$\begin{aligned} u\frac{\partial u}{\partial x} + v\frac{\partial u}{\partial y} + w\frac{\partial u}{\partial z} &= \left(1 + \tfrac{1}{\beta}\right)\frac{\mu_{nf}}{\rho_{nf}}\frac{\partial^2 u}{\partial z^2} - \frac{\sigma_{nf}B_0^2}{\rho_{nf}}u - \frac{\mu_{nf}}{\rho_{nf}}\frac{1}{K}u \\ &+ g_{nf}\beta_T(T - T_\infty) + g_{nf}\beta_C(C - C_\infty) \end{aligned} \tag{3}$$

$$u\frac{\partial v}{\partial x} + v\frac{\partial v}{\partial y} + w\frac{\partial v}{\partial z} = \left(1 + \frac{1}{\beta}\right)\frac{\mu_{nf}}{\rho_{nf}}\frac{\partial^2 v}{\partial z^2} - \frac{\sigma_{nf}B_0^2}{\rho_{nf}}v - \frac{\mu_{nf}}{\rho_{nf}}\frac{1}{K}v \tag{4}$$

(5)

$$u\frac{\partial T}{\partial x}+v\frac{\partial T}{\partial y}+w\frac{\partial T}{\partial z}=k_{nf}\frac{\partial^2 T}{\partial z^2}-\frac{1}{\rho C_\rho}\frac{\partial q_r}{\partial z}+\frac{\mu_{nf}}{(\rho C_\rho)}\left[\left(\frac{\partial u}{\partial z}\right)^2+\left(\frac{\partial v}{\partial z}\right)^2\right]+\frac{\sigma_{nf}B_0^2}{\rho_{nf}}u^2$$
$$+\tau\left\{D_B\left(\frac{\partial T}{\partial z}\frac{\partial C}{\partial z}\right)+\frac{D_T}{T_\infty}\left(\frac{\partial T}{\partial z}\right)^2\right\}+\frac{Q}{\rho C_\rho}\left(T-T_\infty\right)+q'''$$

(6)

$$u\frac{\partial C}{\partial x}+v\frac{\partial C}{\partial y}+w\frac{\partial C}{\partial z}=D_B\frac{\partial^2 C}{\partial z^2}+\frac{D_T}{T_\infty}\frac{\partial^2 T}{\partial z^2}$$

The associated boundary conditions are as follows:

(7)

$$u=ax+\gamma\frac{\partial u}{\partial z},\ v=by+\gamma\frac{\partial v}{\partial z},\ w=0,\ \ -k\frac{\partial T}{\partial z}=n_f\left(T_f-T\right),$$
$$-D_B\frac{\partial C}{\partial z}=n_s\left(C_s-C\right),\ \ z=0;$$
$$u\to 0,\ v\to 0,\ T\to T_\infty,\ C\to C_\infty,\ as\ z\to\infty$$

There is no lateral motion at $z\to\infty$, where $n_f$is the convective heat transfer coefficient, n_S is the convective mass transfer coefficient and T_f and C_S are the convective fluid temperature and concentration below the moving sheet.

(8)

$$\frac{\partial q_r}{\partial z}=\frac{-4\sigma^*}{3\kappa^*}\frac{\partial T^4}{\partial z}\equiv\frac{-16\sigma^* T_S^3}{\partial z^2}\frac{\partial^2 T}{\partial z^2}$$

Using Rosseland's approximation [21] & [22], where u, v and w are the velocity components in x, y and z-direction respectively $\beta=\mu_B\sqrt{2\pi_c/P_Z}$ is the Casson fluid parameter, B is the magnetic induction, $(\rho C_\rho)_{n_f}$ is the heat capacity of the nanofluid particle, $(\rho C_\rho)_f$ is the heat capacity of the base fluid, $\rho_{n_f}$is the nanofluid density, ρ_f is the base fluid density, σ_{n_f}Electrical conductivity of the nanofluid, κ_{n_f} is the thermal conductivity of the nanofluid, $U_{n_f}$is the dynamic viscosity of the nanofluid, σ^*, κ^* are the symbols used for the absorption coefficient and the Stefan Boltzmann constant respectively. In order to transform the set of equations (2) to (7) the following similarity variables are introduced [23] & [24]:

(9)

$$u=axf'(\eta),v=byg'(\eta),w=-(av)^{1/2}(f+g)(\eta),\eta=\sqrt{\frac{a}{v}}z,$$
$$\theta(\eta)=\frac{T-T_\infty}{T_w-T_\infty},h(\eta)=\frac{c-c_\infty}{c_w-c_\infty}$$

$f(\eta)$ and $g(\eta)$ are dimensionless velocity along $x$and$y$direction respectively $\theta(\eta)$ is the dimensionless temperature and $h(\eta)$ is the dimensionless concentration. The important parameters in this problem are defined as follows:

(10)

$$M=\frac{\sigma_{nf}B_0^2}{a\rho_{nf}},K_1=\frac{v_f}{aK},R=\frac{4\delta^*T_\infty^3}{k^*k_{nf}},\quad Nb=\frac{\tau D_B\left(C_w-C_\infty\right)}{k_{nf}},Nt=\frac{\tau D_B\left(T_w-T_\infty\right)}{aK},$$

$$\Pr=\frac{v_f}{k_{nf}}(10)B_{it}=\frac{v_f}{k}\left(\frac{v_f}{a}\right)^{\frac{1}{2}},\ B_{ic}=\frac{n_s}{D_B}\left(\frac{v_f}{a}\right)^{\frac{1}{2}},Ec_x=\frac{a^2x^2}{\rho C_p\left(T_w-T_\infty\right)},$$

$$Ec_y = \frac{b^2y^2}{\rho C_p\left(T_w - T_\infty\right)}, \delta = \frac{Q}{a\rho C_p}$$

(11) $$Gr = \frac{g_{nf}\beta_T}{a^2x}\left(T_w - T_\infty\right),\ s = \frac{b}{a},\ \ Gs = \frac{g_{nf}\beta_C}{a^2x}\left(C_w - C_\infty\right)$$

The physical quantities of engineering interest are the local skin friction coefficient in x and y directions, the Nusselt number which represents the Fourier rate of heat transfer at the surface of the sheet and Sherwood number which denotes the Hicks rate of mass transfer at the surface of the sheet. These quantities are defined as follows;

(12)
$$C_{fx} = \frac{\tau_{wx}}{\rho u_w^2},\quad C_{fy} = \frac{\tau_{wy}}{\rho v_w^2},\quad \tau_{wx} = \mu\left(\frac{\partial u}{\partial z}\right)_{z=0},\quad \tau_{wy} = \mu\left(\frac{\partial v}{\partial z}\right)_{z=0}$$

(13) $$Nu_x = \frac{xq_w}{k\left(T_w - T_\infty\right)},\quad Sh_x = \frac{x_{qm}}{D_B\left(C_w - C_\infty\right)}$$

(14)
$$q_w = -\left(k_f + \frac{4R}{3}\right)\left(\frac{\partial T}{\partial z}\right)_{z=0},\qquad q_m = -D_B\left(\frac{\partial C}{\partial z}\right)_{z=0}$$

τ_{wx} and τ_{wy} are the wall shear stress along x and y– directions respectively $q_w$and q_m are the heat flux and mass flux at the surface respectively. Applying similarity variables to the concentration terms in equation (12) and the Nusselt number and Sherwood numbers parameters in equation (13), we have

(15)
$$C_{fx}Re^{1/2} = \left(1 + \frac{1}{\beta}\right)f''(0),\qquad C_{fy}Re^{1/2} = \left(1 + \frac{1}{\beta}\right)g''(0)(16)Nu_xRe^{1/2}$$

$$= -\left(1 + \frac{4R}{3}\right)\theta'(0),\qquad Sh_xRe^{1/2} = -h'(0)$$

where $Re = \frac{u_w x}{v_f}$ is the local Reynolds number based on the stretching velocity. Using the relation in equation (9) alongside the equations (10-17), equation (2) is identically satisfied [23] & [24] and consequently using the assumption that $f' = r$ and $g' = t$, to reduce the order of nonlinear differential equations, the system of equations (3)-(6) becomes;

(16)
$$\left(1 + \frac{1}{\beta}\right)r''(\eta) + (f(\eta) + sg(\eta))r'(\eta) - (r(\eta))^2 - r(\eta)\left(M + K_1\right) + Gr\theta(\eta) + Gsh(\eta) = 0$$

(17) $$\left(1 + \frac{1}{\beta}\right)t''(\eta) + (f(\eta) + sg(\eta))t'(\eta) - t(\eta)\left(M + K_1\right) - (t(\eta))^2 = 0$$

(18)
$$(1+\tfrac{4R}{3})\theta''(\eta)+\Pr(f(\eta)+sg(\eta))\theta'(\eta)+Nt\left(\theta'(\eta)\right)^2+Nb\theta'(\eta)h'(\eta)$$
$$+M\Pr\left[Ec_x\left(f'(\eta)\right)^2+Ec_y\left(g'(\eta)\right)^2\right]+\Pr\left[Ec_x\left(f''(\eta)\right)^2+Ec_y\left(g''(\eta)\right)^2\right]$$
$$+\delta\Pr\theta(\eta)+\left[A^*f'(\eta)+B^*\theta(\eta)\right]=0$$

(19) $$h''(\eta)+Sc\left(f(\eta)+sg(\eta)\right)h'(\eta)+S_0\theta''(\eta)=0$$

and the corresponding boundary conditions becomes the following

(20) $$f(0)=0,\quad r(0)=1+\gamma r'(0),\quad g(0)=0,\quad t(0)=1+\gamma t'(0)$$

(21) $$\theta'(0)=-B_{it}(1-\theta(0)),\quad h'(0)=-B_{ic}(1-h(0))\quad at\eta=0,$$

(22) $$r(\infty)\to 0,\quad t(\infty)\to 0,\quad \theta(\infty)\to 0,\quad h(\infty)\to 0$$

3. Method of Solution

The exact analytical solutions for the set of non-linear ordinary differential equations (16) – (19), alongside with boundary conditions are not possible. Hence, this system of nonlinear differential equations is solved by employing a numerical method, the Finite Element Method (FEM). This method has been studied for a wide range of non-linear problems by various Scholars ([21] & [23]-[25]). The variational form associated with equations (16) – (19), together with the assumption equations over a typical element over a two -nodded linear element (η_e,η_{e+1}), is given as following;

(23) $$\int_{\eta_e}^{\eta_{e+1}} N_1\left[f'(\eta)-r\right]d\eta=0(25)\int_{\eta_e}^{\eta_{e+1}} N_2\left[g'(\eta)-t\right]d\eta=0$$

(24)
$$\int_{\eta_e}^{\eta_{e+1}} N_3[(1+\tfrac{1}{\beta})r''(\eta)+(f(\eta)+Sg(\eta))r'(\eta)-(r(\eta))^2$$
$$-r(\eta)(M+K_1)+Gr\theta(\eta)+Gsh(\eta)]d\eta=0$$

(25) $$\int_{\eta_e}^{\eta_{e+1}} N_4[(1+\frac{1}{\beta})t''(\eta)+(f(\eta)+Sg(\eta))t'(\eta)-(t(\eta))^2-t(\eta)(M+K_1)]d\eta=0$$

(26)
$$\int_{\eta_{e+1}}^{\eta_{e+1}} N_5[(1+\frac{4R}{3})\theta''(\eta)+\Pr(f(\eta)+sg(\eta))\theta'(\eta)+Nt\left(\theta'(\eta)\right)^2+Nb\theta'(\eta)h'(\eta)$$
$$+M\Pr\left[Ec_x\left(f'(\eta)\right)^2+Ec_y\left(g'(\eta)\right)^2\right]+\Pr\left[Ec_x\left(f''(\eta)\right)^2+Ec_y\left(g''(\eta)\right)^2\right]$$
$$+\delta\Pr\theta(\eta)+\left[A^*f'(\eta)+B^*\theta(\eta)\right]]d\eta=0$$

(27) $$\int_{\eta_{e+1}}^{\eta_{e+!}} N_6[h''(\eta)+Sc\left(f(\eta)+sg(\eta)\right)h'(\eta)+S_0\theta''(\eta)]d\eta=0$$

where N_1, N_4, N_3, N_4, N_5 and N_6 are the weight functions and may be viewed as the variation in f, r, g, t, θ and h respectively. The finite element model may be obtained from equations (23) - (27) by substituting finite element approximation of the form:

(28)
$$f = \sum_{i=1}^{2} f_j\psi_j, r = \sum_{i=1}^{2} r_j\psi_j, g = \sum_{i=1}^{2} g_j\psi_j, t = \sum_{i=1}^{2} t_j\psi_j, \theta = \sum_{i=1}^{2} \theta_j\psi_j, h = \sum_{i=1}^{2} h_j\psi_j$$

Incorporating the boundary conditions directly in the strong form as presented in equation (23) – (27) is a daunting task. Also, the requirement on continuity of field variables is much stronger in its present forms. In order to overcome the difficulties, weak formulations are preferred. The weak formulations help to reduce the order of continuity needed for the elements selected i.e. it will reduce the continuity requirements on the basis approximation functions thereby allowing the use of easy to construct and implement polynomials, moreover, weak formulation automatically enforces natural boundary conditions. Substituting equation (28) into the equations (23)-(24), and the weak forms of equations (25)-(27), we obtained:

(29)
$$\int_{\eta_e}^{\eta_{e+1}} \psi_i[\sum_{j=1}^{2} \psi_j' f_j - \sum_{j=1}^{2} \psi_j r_j]d\eta = 0$$

(30)
$$\int_{\eta_e}^{\eta_{e+1}} \psi_i[\sum_{j=1}^{2} \psi_j' g_j - \sum_{j=1}^{2} \psi_j t_j]d\eta = 0$$

(31)
$$(1+\tfrac{1}{\beta})[\psi_i \textstyle\sum_{j=1}^{2} \psi_j' r_j \big|_{\eta_e}^{\eta_{e+1}} - \int_{\eta_e}^{\eta_{e+1}} \psi_i' \sum_{j=1}^{2} \psi_j' r_j d\eta] + \int_{\eta_e}^{\eta_{e+1}} \psi_i[\sum_{j=1}^{2} \psi_j' r_j(\sum_{j=1}^{2} \psi_j f_j + \sum_{j=1}^{2} \psi_j g_j) - (\sum_{j=1}^{2} \psi_j r_j)^2 - \sum_{j=1}^{2} \psi_j r_j(M+K_1)]d\eta = 0$$

(32)
$$(1+\tfrac{1}{\beta})[\psi_i \textstyle\sum_{j=1}^{2} \psi_j' t_j \big|_{\eta_e}^{\eta_{e+1}} - \int_{\eta_e}^{\eta_{e+1}} \psi_i' \sum_{j=1}^{2} \psi_j' t_j d\eta] + \int_{\eta_e}^{\eta_{e+1}} \psi_i[\sum_{j=1}^{2} \psi_j' t_j(\sum_{j=1}^{2} \psi_j f_j + \sum_{j=1}^{2} \psi_j g_j) - (\sum_{j=1}^{2} \psi_j t_j)^2 - \sum_{j=1}^{2} \psi_j t_j(M+K_1)]d\eta = 0$$

(33)
$$(1+\tfrac{1}{\beta})[\psi_i \textstyle\sum_{j=1}^{2} \psi_j' \theta_j \big|_{\eta_e}^{\eta_{e+1}} - \int_{\eta_e}^{\eta_{e+1}} \psi_i' \sum_{j=1}^{2} \psi_j' \theta_j d\eta] + \int_{\eta_e}^{\eta_{e+1}} \psi_i[\sum_{j=1}^{2} \psi_j' \theta_j P_r(\sum_{j=1}^{2} \psi_j f_j + \sum_{j=1}^{2} \psi_j g_j) + N_t(\sum_{j=1}^{2} \psi_j t_j)^2 + N_b \sum_{j=1}^{2} \psi_j \theta_j \sum_{j=1}^{2} \psi_j h_j + E_c(\sum_{j=1}^{2} \psi_j r_j)^2]d\eta = 0$$

(34)
$$(\psi_i \textstyle\sum_{j=1}^{2} \psi_j' h_j \big|_{\eta_e}^{\eta_{e+1}} - \int_{\eta_e}^{\eta_{e+1}} \psi_i' \sum_{j=1}^{2} \psi_j' h_j d\eta + \int_{\eta_e}^{\eta_{e+1}} \psi_i[\sum_{j=1}^{2} \psi_j' h_j L_e(\sum_{j=1}^{2} \psi_j f_j + \sum_{j=1}^{2} \psi_j g_j)]d\eta + \tfrac{N_t}{N_b}[\psi_i \textstyle\sum_{j=1}^{2} \psi_j' \theta_j \big|_{\eta_e}^{\eta_{e+1}} - \int_{\eta_e}^{\eta_{e+1}} \psi_i' \sum_{j=1}^{2} \psi_j' \theta_j d\eta] = 0$$

The finite element model of the equations for the e^{th} element thus formed is given in matrix form as follows:

$$(35)\qquad \begin{pmatrix} [K^{11}] & [K^{12}] & [K^{13}] & [K^{14}] & [K^{15}] & [K^{16}] \\ [K^{21}] & [K^{22}] & [K^{23}] & [K^{24}] & [K^{25}] & [K^{26}] \\ [K^{31}] & [K^{32}] & [K^{33}] & [K^{34}] & [K^{35}] & [K^{36}] \\ [K^{41}] & [K^{42}] & [K^{43}] & [K^{44}] & [K^{45}] & [K^{46}] \\ [K^{51}] & [K^{52}] & [K^{53}] & [K^{54}] & [K^{55}] & [K^{56}] \\ [K^{61}] & [K^{62}] & [K^{63}] & [K^{64}] & [K^{65}] & [K^{66}] \end{pmatrix} \begin{Bmatrix} f^e \\ r^e \\ g^e \\ t^e \\ \theta^e \\ h^e \end{Bmatrix} = \begin{Bmatrix} S^{1e} \\ S^{2e} \\ S^{3e} \\ S^{4e} \\ S^{5e} \\ S^{6e} \end{Bmatrix}$$

where $[K^{mn}]$ are set of matrices, while $\{f^e\},\{r^e\},\{g^e\},\{t^e\},\{\theta^e\},\{h^e\} and \{S^{me}\}$ are associated vectors, for $m,n=1,2,3,4,5,6$ are all defined as follows:

$$K_{ij}^{11}=\int_{\eta_e}^{\eta_{e+1}}\psi_i\psi_j'd\eta,\quad K_{ij}^{12}=-\int_{\eta_E}^{\eta_{E+1}}\psi_i\psi_j d\eta,\quad K_{ij}^{13}=K_{ij}^{14}=K_{ij}^{15}=K_{ij}^{16}=0$$

$$K_{ij}^{21}=K_{ij}^{22}=K_{ij}^{25}=K_{ij}^{26}=0,\quad K_{ij}^{23}=\int_{\eta_e}^{\eta_{e+1}}\psi_i\psi_j'd\eta,\quad K_{ij}^{24}=-\int_{\eta_E}^{\eta_{E+1}}\psi_i\psi_j d\eta,$$

$$K_{ij}^{31}=K_{ij}^{33}=K_{ij}^{34}=0\qquad K_{ij}^{32}=-\left(1+\frac{1}{\beta}\right)\left\{\int_{\eta_e}^{\eta_{e+1}}\psi_i'\psi_j'd\eta\right\}+$$

$$\int_{\eta_e}^{\eta_{e+1}}\left[\psi_i\psi_j'\left(\sum_{j-1}^{2}\psi_j f_j+s\sum_{j-1}^{2}\psi_j g_j\right)-(M+K_1)\,\psi_i\psi_j-\bar{r}\psi_j'\psi_j'\right]d\eta$$

$$K_{ij}^{35}=Gr\int_{\eta_E}^{\eta_{E+1}}\psi_i\psi_j d\eta,\quad K_{ij}^{36}=Gs\int_{\eta_E}^{\eta_{E+1}}\psi_i\psi_j d\eta,$$

$$K_{ij}^{41}=K_{ij}^{42}=K_{ij}^{43}=K_{ij}^{45}=K_{ij}^{46}=0K_{ij}^{44}=-\left(1+\frac{1}{\beta}\right)\left\{\int_{\eta_e}^{\eta_{e+1}}\psi_i'\psi_j'd\eta\right\}+$$

$$\int_{\eta_e}^{\eta_{e+1}}\left[\psi_i\psi_j'\left(\sum_{j-1}^{2}\psi_j f_j+s\sum_{j-1}^{2}\psi_j g_j\right)-(M+K_1)\,\psi_i\psi_j-\bar{h}\psi_j'\psi_j'\right]d\eta$$

$$K_{ij}^{51}=K_{ij}^{53}=K_{ij}^{56}=0,K_{ij}^{52}=\int_{\eta_e}^{\eta_{e+1}}\psi_i\left[Ec_x\bar{r}_j\psi_j+A^*\psi_j\right]d\eta$$

$$K_{ij}^{54}=\int_{\eta_e}^{\eta_{e+1}}\psi_i\left[Ec_y\bar{r}_j\psi_j\right]d\eta\qquad K_{ij}^{55}=-\left(1+\frac{4R}{3}\right)\left\{\int_{\eta_e}^{\eta_{e+1}}\psi_i'\psi_j'd\eta\right\}+$$

$$\int_{\eta_e}^{\eta_{e+1}}\psi_i\left[B^*\psi_j+\Pr\left(\sum_{j-1}^{2}\psi_j f_j+s\sum_{j-1}^{2}\psi_j g_j\right)\psi_j'+\psi_j\left(\delta\Pr+Nbh_j+Nt\bar{\theta}\right)\right]d\eta$$

$$K_{ij}^{61} = K_{ij}^{62} = K_{ij}^{63} = K_{ij}^{64} = 0 K_{ij}^{65} = -\int_{\eta_e}^{\eta_{e+1}} \psi_i' \psi_j' d\eta$$

$$K_{ij}^{66} = -\left\{\int_{\eta_e}^{\eta_{e+1}} \psi_i' \psi_j' d\eta\right\} + \int_{\eta_e}^{\eta_{e+1}} \left[\psi_i \psi_j' Sc \left(\sum_{j-1}^{2} \psi_j f_j + s \sum_{j-1}^{2} \psi_j g_j\right)\right] d\eta$$

$$S^1 = S^2 = 0, S^3 = S^4 = -\left(1 + \frac{1}{\beta}\right)\left\{\psi_i \ \psi_j'\Big|_{\eta_e}^{\eta_{e+1}}\right\}, S^5 = -\left(1 + \frac{4R}{3}\right)\left[\psi_i \ \psi_j'\Big|_{\eta_e}^{\eta_{e+1}}\right]$$

$$S^6 = -\psi_i \ \psi_j'\Big|_{\eta_e}^{\eta_{e+1}} - \frac{Nt}{Nb}\psi_i \ \psi_j'\Big|_{\eta_e}^{\eta_{e+1}}$$

The element matrix given by equation (35) is of the order 12×12 and the whole domain is divided into set of equations a matrix of order 7206×7206 is obtained. The system of equations obtained is nonlinear and therefore an iterative scheme is used for solving it. After applying the boundary conditions, the remaining system of equations is solved. The iterative process is terminated when the following convergence criterion is satisfied $\sum_i \left|\Theta_i^m - \Theta_i^{m-1}\right| \leq 10^{-4}$ where Θ stand for either $f,\ r,\ g,\ t,\ \theta,\ h$ and m denotes the iterative step.

In order to assess the accuracy of the present FEM code, the numerical results have been compared with previously published work, and are reported in Table 1. It can be inferred from the table that there exist an excellent agreement, which testify to the validity of the FEM code.

Table 1: Comparison of local Skin friction coefficients for various physical parameters

		$\left(1+\frac{1}{\beta}\right) f''(0)$			$\left(1+\frac{1}{\beta}\right) g''(0)$		
PP	Values	FEM (Present Study)	RK4 [14]	DIFF= FEM-RK4	FEM (Present Study)	RK4 [14]	DIFF = FEM– RK4
β	1.0	-1.4314	-1.4314	0.000011	-1.59208	-1.5921	0.000044
	2.0	-1.2443	-1.2443	0.000010	-1.34429	-1.3443	0.000033
	3.0	-1.0241	-1.0241	0.000009	-1.12119	-1.1212	0.000021
M	1.0	-1.0568	-1.0568	0.000055	-1.05683	-1.0568	0.000012
	2.0	-1.2036	-1.2037	0.000044	-1.20368	-1.2037	0.000012
	3.0	-1.3347	-1.3347	0.000011	-1.33467	-1.3347	0.000002
Nb	1.0	-1.0568	-1.0568	0.000021	-1.05684	-1.0568	0.000004
	2.0	-1.0568	-1.0568	0.000015	-1.05684	-1.0568	0.000005
	3.0	-1.0568	-1.0568	0.000080	-1.05684	-1.0568	0.000003
Nt	0.5	-1.0568	-1.0568	0.000021	-1.05684	-1.0568	0.000003
	1.0	-1.0568	-1.0568	0.000011	-1.05683	-1.0568	0.000011
	1.5	-1.0568	-1.0568	0.000031	-1.05682	-1.0568	0.000021

Results and Discussion. The effect of velocity slip parameter and Casson fluid parameter on the velocity profile is as shown in Figures 2 and 3. As β increases, the yield stress decreases thereby reducing the velocity profile. Due to the slip condition, the velocity near the sheet is no longer equal to the stretching velocity of the sheet. The fluid velocity decreases because under the slip condition, the pulling of the stretching sheet can only be transmitted to the fluid and the velocity decreases with the slip parameter. Therefore increasing value of Slip and Casson parameter decreases the velocity boundary layer thickness. Figures 4 and 5 shows the effect of Thermal Grashof (Gr) and Solutal Grashof number (Gs) on the velocity profile. As the magnitude of Gr and Gs increases, the velocity profile is accelerated due to the enrichment of the buoyancy force. The effect of Magnetic Parameter on the velocity profile is illustrated in Figure 6. The presence of a magnetic field introduces a retarding force, known as Lorentz force which slow down the fluid velocity.

Figure 7 shows the effect of Prandtl Number on the temperature profile. An increase in Prandtl number leads to a decrease in the temperature profile. In heat transfer problems, the Prandtl number controls the thickness of the momentum and thermal boundary layer. Fluids with lower Prandtl number have higher thermal conductivities so that heat can diffuse from the sheet faster for higher Prandtl fluid.

Figures 8 and 9 shows the effect of Brownian motion and thermophoresis on the temperature profile. It shows that the fluid temperature increases as Brownian

motion increases as well as thermophoresis parameter. The influence of non - uniform heat source/sink parameters on the temperature profile is shown in Figure 10. It is observed that energy is created in the boundary layer as the heat source increases ($A^* > 0$) which implies exothermic reaction and a significantly large amount of heat increase the temperature distribution of the fluid. When ($A^* < 0$) energy is absorbed in the boundary layer. Hence the temperature reduces appreciably with the increasing value of the $A^* < 0$. The influence of the temperature-dependent heat source/sink parameter B^* on the temperature profile shows that energy is given off into the boundary layer for increasing value of $B^*(B^* > 0)$. Hence the thermal boundary layer thickness increases. For ($B^* < 0$), energy is absorbed for increasing value of B^*. Hence the thermal boundary layer thickness as well as the temperature decreases. Figures 11 and 12 shows the effect of Brownian motion parameter and thermophoresis parameter on the concentration profile. It shows that the fluid concentration decreases as Brownian motion increases whereas as well as thermophoresis parameter increases the concentration profile increases. Figure 13 shows the effect of Schmidt Number (Sc) on the concentration profile. It is noticed that the concentration boundary layer thickness decreases as Sc increases. Schmidt number enhanced the mass diffusivity of the system, which reduced the boundary layer thickness of solutal concentration.

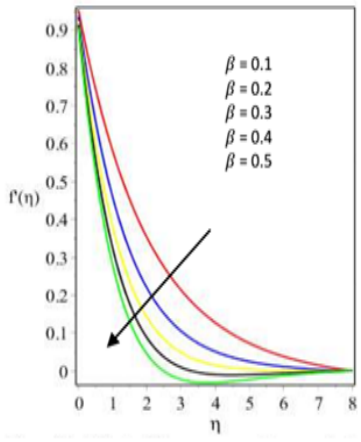


Figure 2a

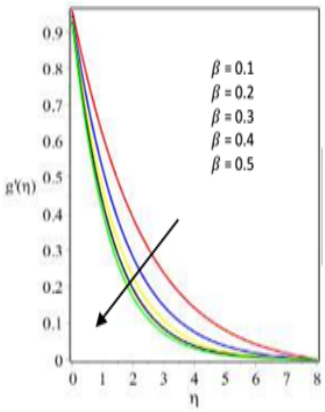


Figure 2b

Figure 2a: Effect of Casson fluid parameter on velocity profile in x–direction
Figure 2b: Effect of Casson fluid parameter on velocity profile in y – direction

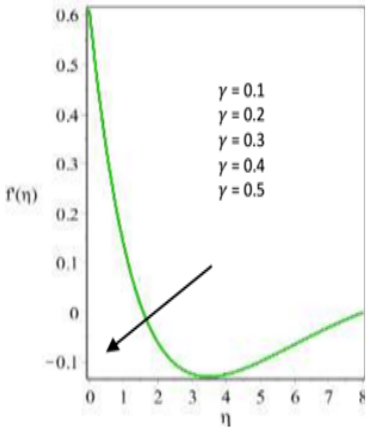


Figure 3a

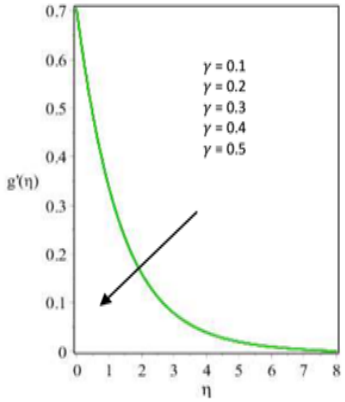


Figure 3b

Figure 3a: Effect of Slip on velocity profile in x – direction
Figure 3b: Effect of Slip on velocity profile in y – direction

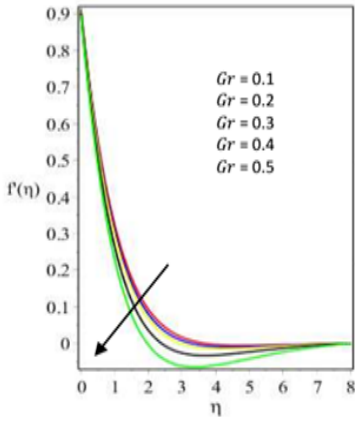


Figure 4a

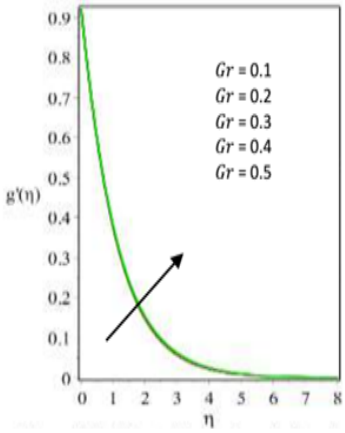


Figure 4b

Figure 4a: Effect of Thermal Grashof number on velocity profile in x – direction
Figure 4b: Effect of Thermal Grashof number on velocity profile in y – direction

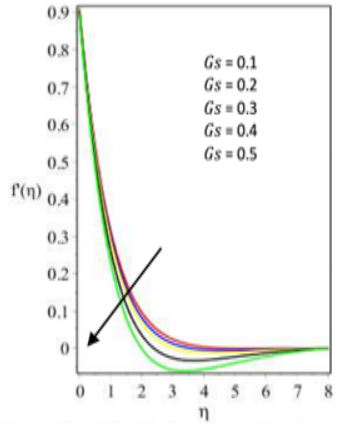


Figure 5a

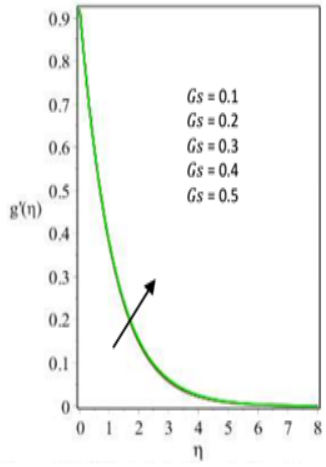


Figure 5b

Figure 5a: Effect of Solutal Grashof number on velocity profile in x – direction
Figure 5b: Effect of Solutal Grashof number on velocity profile in y – direction

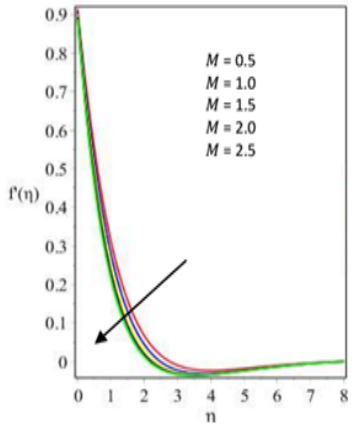


Figure 6a

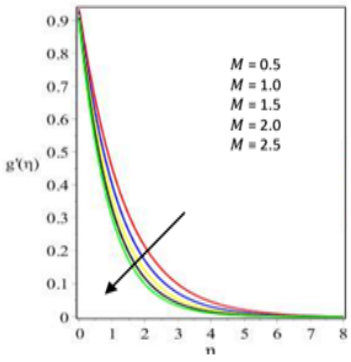


Figure 6b

Figure 6a: Effect of Magnetic Parameter on velocity profile in x – direction
Figure 6b: Effect of Magnetic Parameter on velocity profile in y – direction

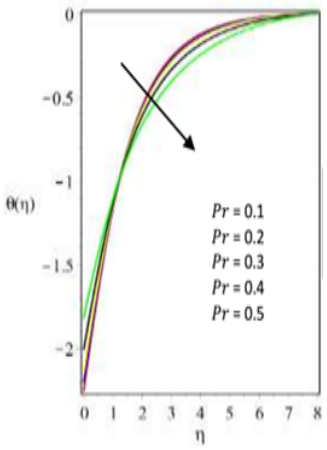


Figure 7

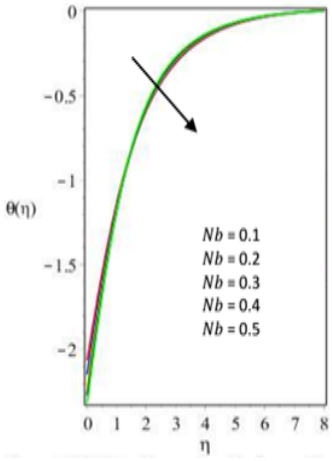


Figure 8

Figure 7: Effect of Prandtl number on temperature profile
Figure 8: Effect of Brownian motion parameter on temperature profile

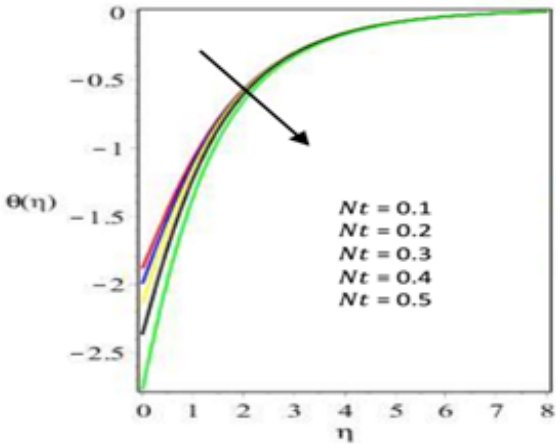


Figure 9: Effect of Thermophoresis parameter on temperature profile

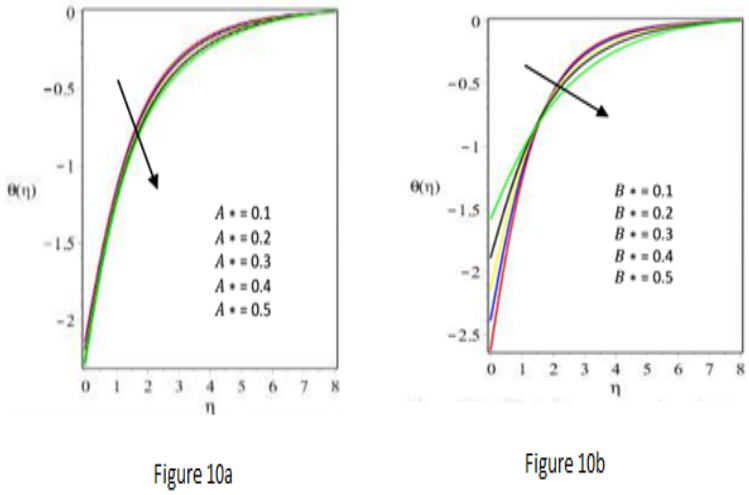


Figure 10a: Effect of Space-dependent non –uniform heat sink on temperature profile

Figure 10b: Effect of Temperature-dependent non –uniform heat sink on temperature profile

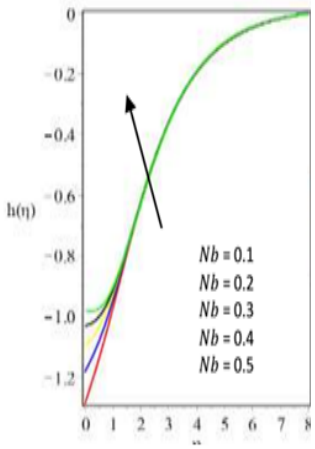


Figure 11

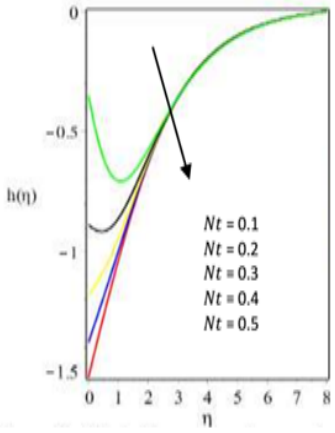


Figure 12

Figure 11: Effect of Brownian motion parameter on concentration profile
Figure 12: Effect of Thermophoresis parameter on concentration profile

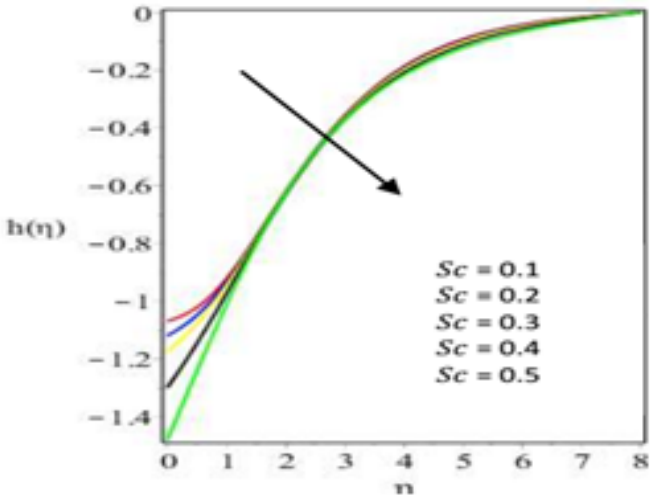


Figure 13: Effect of Schmidt number on concentration profile

Conclusions: In this paper, the effect of Brownian motion and thermophoresis on heat and mass transfer on MHD convective boundary layer flow of Casson fluid over a linearly stretching sheet with velocity slip is considered. The fundamental equations have been solved numerically using Finite Element Method. A comparison of the results obtained in this paper with existing findings shows a very close agreement between the two. Finally, the summary of the aforementioned results are as follows:

(1) The temperature profile increases as the value of Brownian motion and thermophoresis increases. On the other hand, the fluid concentration decreases as Brownian motion increases whereas as well as thermophoresis parameter increases the concentration profile increases.
(2) The higher the value of Casson parameter the lower (reduces) the momentum boundary layer thickness i.e. it decreases momentum boundary layer thickness in turn decreasing the velocity profile of the fluid.
(3) Increase in the value of Schmidt number results in thickness of the boundary layer concentration which is smaller than the thermal boundary layer thickness.
(4) The effect of Prandtl number is to decrease the thermal boundary layer thickness, which is in contrast to the effects of other parameter on heat transfer.

Acknowledgement: The authors are very grateful to University of Lagos for the supports they received during the compilation of this work and to anonymous referees for their careful reading of the paper and helpful suggestions.

Competing interests: The manuscript was read and approved by all the authors. They therefore declare that there is no conflicts of interests regarding this paper.

Funding: The Authors received no financial support for the research, authorship, and/or publication of this article.

References

[1] Shehzad S. A., Hayat T. & Alsaedi A. (2016). Three-Dimensional MHD flow of Casson fluid in porous medium with heat generation. *Journal of Applied Fluid Mechanics*. **9** (1), 215-223.

[2] Sobamowo M. G., Yinusa A. A., Oluwo A. A. & Alozie S. I. (2018). Finite Analysis of Flow and Heat Transfer of Dissipative Casson-Carreau Nanofluid Over a Stretching Sheet Embedded in a Porous Medium. *Aeronautic and Aerospace Open Access Journal*. **2** (5), 294-308.

[3] Mahanta G. & Shaw S. (2015). 3D Casson fluid flow past a porous linearly Stretching Sheet with convective boundary condition. *Alexandria Engineering Journal*. **54**, 653-659.

[4] Nadeem S., IHaq R. U., Akbar N. S. & Khan Z. H. (2013). MHD three-dimensional Casson fluid flow past a porous linearly Stretching Sheet. *Alexandria Engineering Journal*. **52**, 577-582.

[5] Patel H. R. (2019). Effects of Cross diffusion and Heat generation in mixed convective (MHD) flow of Casson fluid through Porous Medium with Nonlinear Thermal Radiation. *Heliyon*. 1-26.

[6] Fatunmbi E. O. & Odesola A. S. (2018). MHD Free Convective Heat and Mass Transfer of a Micropolar Fluid Flow Over a Stretching Permeable Sheet with Constant Heat and Mass Flux. *Asian Research Journal of Mathematics*. **9** (3), 1-15.

[7] Chen J., Liang C. & Lee J. D. (2011). Theory and Simulation of Micropolar Fluid Dynamics. *Journal of Nanoengineering and Nanosystemss*. **224**, 31-39.

[8] Olajuwon B. I., Oahimire J. I. & Abiala I. O. (2012). Heat and Mass Transfer in a Micropolar Fluid in the presence of Thermal Radiation and Chemical Reaction. *Journal of the Nigerian Association of Mathematical Physics*. **22**, 465-482.

[9] Oahimire J. I., Olajuwon B. I., Waheed M. A. & Abiala I. O. (2013). Analytical solution to MHD Micropolar fluid flow past a vertical plate in a slip-flow regime in the presence of Thermal Diffusion and Thermal Radiation. *Journal of the Nigerian Mathematical Society*. **32**, 33-60.

[10] Fenuga O. J., Abiala I. O. & Salawu S. O. (2018). Analysis of thermal boundary layer flow over a vertical plate with electrical conductivity and convective surface boundary conditions. International Journal of Physical Sciences. **17** (2), 1-9.

[11] Freidoonimehr N. & Rahimi A. B. (2018). Brownian motion effect on heat transfer of a three-dimensional nanofluid flow over a stretched sheet with velocity slip. *Journal of Thermal Analysis and Calorimetry*. **135** 10.1007/s10973-018-7060-y.

[12] Shateyi S. (2017). Numerical Analysis of Three-Dimensional MHD Nanofluid Flow over a Stretching Sheet with Convective Boundary Conditions Through a Porous Medium. *Nanofluid Heat and Mass Transfer in Engineering Problem*. Intech Open Chapter **1**, 1-22.

[13] Zaigham-Zia Q. M., Ullah I., Waqas M., Alsaedi A. & Hayat T. (2018). Cross diffusion and exponential space dependent heat source impacts in radiated three-dimensional (3D) flow of Casson fluid by heated surface. *Results in Physics*. **8**, 1275-1282.

[14] Benazir A. J. M., Sivaraj R. & Makinde O. D. (2015). Unsteady MHD Casson fluid flow over a vertical cone and flat plate with non-uniform heat source/sink. *International Journal of Engineering Research in Africa*. **21**, 69-83.

[15] Khalid A., Khan I., Khan A. & Shafie S. (2015). Unsteady MHD Free Convection Flow of Casson Fluid Past over an Oscillating Vertical Plate Embedded in a Porous Medium. *Engineering Science and Technology, an International Journal*. **18** (3), 309-317.

[16] Thammanna G. T., Ganesh Kumar K., Gireesha B. J., Ramesh G. K. & Prasannakumara B. C. (2017). Three dimensional MHD Flow of couple stress Casson fluid past an unsteady stretching surface with chemical reaction. *Results in Physics*. **7**, 4104-4110.

[17] Sulochana C., Payad S. S. & Sandeep N. (2016). Non-uniform heat source or sink effect on the flow of 3D Casson fluid in the presence of Soret and Thermal radiation. *International Journal of Engineering Research in Africa*. **20**, 112-129.

[18] Kalyani K., Sreelakshmi K. & Sarojamma G. (2017). The three-dimensional flow of a non-Newtonian fluid over a flat surface through a porous medium with surface convective conditions. *Global Journal of Pure and Applied Mathematics*. **13**, 2193-2211.

[19] Mondal R. K., Reze-E-Rabbi S., Gharami P. P., Ahmmed S. F. & Arifuzzaman S. M. (2019). A Simulation of Casson Fluid Flow with Variable Viscosity and Thermal Conductivity Effects. *Mathematical Modelling of Engineering Problems*. **6** (4), 625-633.

[20] Renuka P., Ganga B., Kalawanan R. & Abdulhakeem A. K. (2020). Slip Effects in Ohmic Dissipative Non-Newtonian Fluid Flow in the Presence of Aligned Magnetic Field. *Journal of Applied and Computational Mechanics*. **6** (2), 296-306.

[21] Swapna G., Kumar L., Rana P., Kumari A. & Singh B. (2017). finite element study of radiative double-diffusive mixed convection magneto-micropolar flow in a porous medium with chemical reaction and convective condition. *Alexandria Engineering Journal*. 1-4.

[22] Kumar L. (2009). Finite element analysis of combined heat and mass transfer in hydromagnetic micropolar flow along a stretching sheet. *Computational Material Science*. **46**. 841-848.

[23] Reddy S. P., Sreedevi P. & Chamkha A. J. (2017). MHD boundary layer flow, heat and mass transfer analysis over a rotating disk through porous medium saturated by Cu-water and Ag-water nanofluid with Chemical Reaction. *Powder Technol*. **307**, 46-55.

[24] Odesola A. S., Abiala I. O., Akinpelu F. O. & Fenuga O. J. (2020). Analysis of magneto-hydrodynamic (MHD) nanofluid flow with heat and mass transfer over a porous stretching sheet. *International Journal of Applied Mechanics and Engineering*. **25** (4), 162-174.

[25] Abiala I. O. & Gbadeyan J. A. (2015). Finite element dynamic analysis of non-uniform beams on variable one-parameter foundation subjected to uniformly distributed moving loads. *International Journal of Applied Mechanics and Engineering*. **20** (4), 693-715.